minerals

MDPI

Article

Design and Application of a Deep-Sea Engineering Geology In Situ Test System

Kaiming Zhong [1,2], Ming Chen [1,*], Chao Xie [1], Jinrong Zheng [1], Wei Chen [1], Wen Ou [1] and Chunliang Yu [1]

[1] Institute of Deep Sea Science and Engineering, Chinese Academy of Sciences, Sanya 572000, China
[2] University of Chinese Academy of Sciences, Beijing 101408, China
* Correspondence: chenm@idsse.ac.cn

Abstract: Seabed soil layer composed of soft sediments, which has a high water content, low bulk density and low shear strength, has great influence on deep-sea engineering devices. Therefore, accurate measurement of the mechanical properties of seabed sediments is a prerequisite for the construction and safe operation of deep-sea projects. In this study, a deep-sea engineering geology in situ test system was developed to measure cone resistance, sleeve friction, pore pressure and shear resistance in seafloor sediments. The system was tested on land, and the feasibility of the system was verified. We conducted sea trials in the South China Sea and acquired datasets from five stations. The data were analyzed using the Eslami–Fellenius soil classification map, and the soil classification of the site was obtained. The obtained values of cone resistance, sleeve friction, pore pressure and shear resistance can provide mechanical data support for deep-sea engineering in this area.

Keywords: sediment; in situ test; cone resistance; sleeve friction; pore pressure; shear resistance; Eslami–Fellenius soil classification map

check for updates

Citation: Zhong, K.; Chen, M.; Xie, C.; Zheng, J.; Chen, W.; Ou, W.; Yu, C. Design and Application of a Deep-Sea Engineering Geology In Situ Test System. *Minerals* **2023**, *13*, 184. https://doi.org/10.3390/min13020184

Academic Editor: Mamadou Fall

Received: 23 November 2022
Revised: 21 January 2023
Accepted: 23 January 2023
Published: 27 January 2023

Copyright: © 2023 by the authors. Licensee MDPI, Basel, Switzerland. This article is an open access article distributed under the terms and conditions of the Creative Commons Attribution (CC BY) license (https://creativecommons.org/licenses/by/4.0/).

1. Introduction

The deep sea contains rich resources in terms of biology, chemistry, minerals, energy and so on. The effective exploitation of deep-sea resources can promote the economic development of China and improve its comprehensive strength [1–4]. The exploitation of deep-sea resources requires the support of mature deep-sea engineering technology. Mining crawlers, pipelines and anchoring foundations in marine engineering are mainly laid on the soft-soil layer of the seabed [5,6], which is mostly composed of unconsolidated sediments deposited by fine particles over a long time. Such sediments have a high water content, low bulk density and low shear strength [7–9]. Therefore, accurate measurement of the mechanical properties of seabed sediments has become an important prerequisite for the safety of deep-sea engineering construction and operation.

The most commonly used in situ methods for determining the mechanical properties of seabed sediments include the cone penetration test and cross-plate shear test [10–12]. The cone penetration test (CPT) or the cone penetration test with pore pressure measurement (CPTu) can be used to evaluate the division of soil layer and soil character identification of marine thin soft soil. Based on the differences in detection methods, the CPT can be divided into the down-hole CPT and seabed CPT [10,11,13]. The down-hole CPT uses a cyclic propulsion method combining drilling and static penetration, which means that the soil layer that has been penetrated is swept away before the next penetration [14,15]. A typical example of the down-hole CPT is Furgo's Wison–APB system, with a water depth of 3000 m [14]. However, using the down-hole CPT requires drilling prior to detection, which inevitably disturbs the seabed soil; hence, its measurement result is not as accurate as that of the seabed CPT. The seabed CPT works differently from the down-hole CPT, involving continuous penetration of the probe into the soil from the seabed surface through the probe rod [13]. As shown in Figure 1 [16–18], among the internationally known seabed

CPTs are: Vandenberg DW-ROSON100, which has a working water depth of 4000 m and 50 m penetration depth; Fugro SEACALF [19], which has a 4000 m working water depth; NEPTUNE 5000 from Datem Company, UK, which has a 3000 m working water depth and 20 m penetration depth; Geomil's MANTA-200, which has a 2000 m working water depth. The representative device of domestic offshore static penetration technology is described as follows. In 1973, the Institute of Oceanology, Chinese Academy of Sciences, designed a submerged and released underwater static probe with a maximum working depth of 50 m [20,21]. In 2005, the Institute of Engineering Technology of Jilin University developed the "submarine static contact detection test system in shallow sea area", with a maximum working water depth of 55 m [22,23]. In 2005, the Guangzhou Marine Geological Survey developed a marine static probing device with a hydraulic propulsion system in the tube as a key technology. Its working water depth can reach 100 m [24,25].The PeneVector Seabed Static Penetration System, independently developed by Wuhan PENESON Geological Prospecting Technology Company in 2017, has a maximum working water depth of 1480 m [24,26,27].

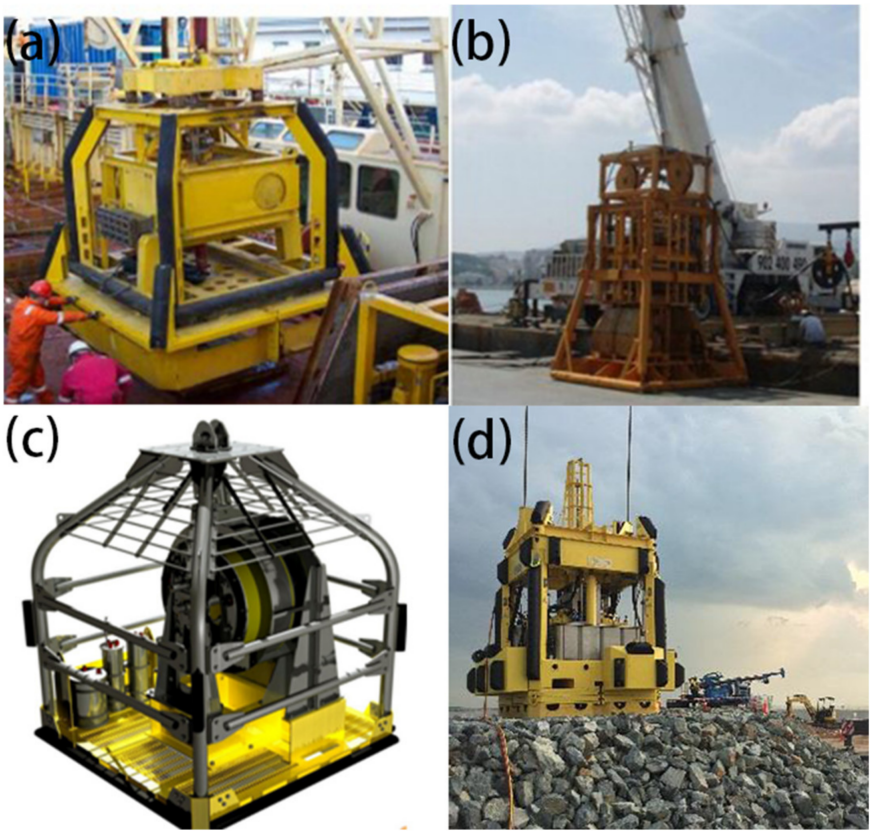


Figure 1. Photographs of seabed CPT (**a**) DW-ROSON100, (**b**) SEACALF, (**c**) NEPTUNE5000 [24], (**d**) MANTA-200.

At present, seafloor in situ detection systems based on sediment mechanical parameters are widely used worldwide, and a large number of measured data and empirical formulas have been accumulated, although there have been relatively few applications in China [5,17,28–30]. Most of the equipment is used for in situ detection via static sounding for marine engineering geological exploration (at a water depth less than 2500 m), and some equipment is used for in situ detection of the geomechanical parameters of shallow surface sediment for deep-sea polymetallic nodule development (at a water depth less than 6000 m) [31–34]. There are no in situ data on mechanical parameters below 3000 m in China. Therefore, in view of the need to determine the mechanical properties of deep-sea thin, soft-soil deposits, we developed a deep-sea engineering geology in situ test system

with a CPT and cross-shear device, and the data obtained by the system filled this gap. The above domestic equipment is equipped with static penetration or cross-shear devices, but does not carry both [34–36]. The CPT and the cross-shear device were both installed on this device, which improved the efficiency of soil mechanic parameter testing of seabed sediments. Furthermore, we carried out research and development and application of CPT digital probe technology under an extremely high pressure environment of 6000 m water depth [37].

2. Design of Deep-Sea Engineering Geology in Situ Test System

The deep-sea engineering geology in situ test system is mainly composed of the following two parts: a remote monitoring platform located on the scientific research ship and a deep-sea engineering geology in situ test device located on the seabed. As shown in Figure 2, the device adopts the seabed operation mode of deck remote control. During deep-sea operation, the scientific research ship supplies power and lowers and recovers the deep-sea engineering geology in situ test device through a photoelectric composite umbilical cable. Under the control of the remote monitoring platform, the device successively implants the digital CPTu and the cross-shear device in seabed sediments. Then, it continuously collects the cone resistance, sleeve friction and pore pressure signals during the penetration process and collects the resistance during the rotation of the cross-shear plate at different depths. The collected data are transmitted back to the remote monitoring platform of the scientific research ship in real time through the photoelectric composite umbilical cable.

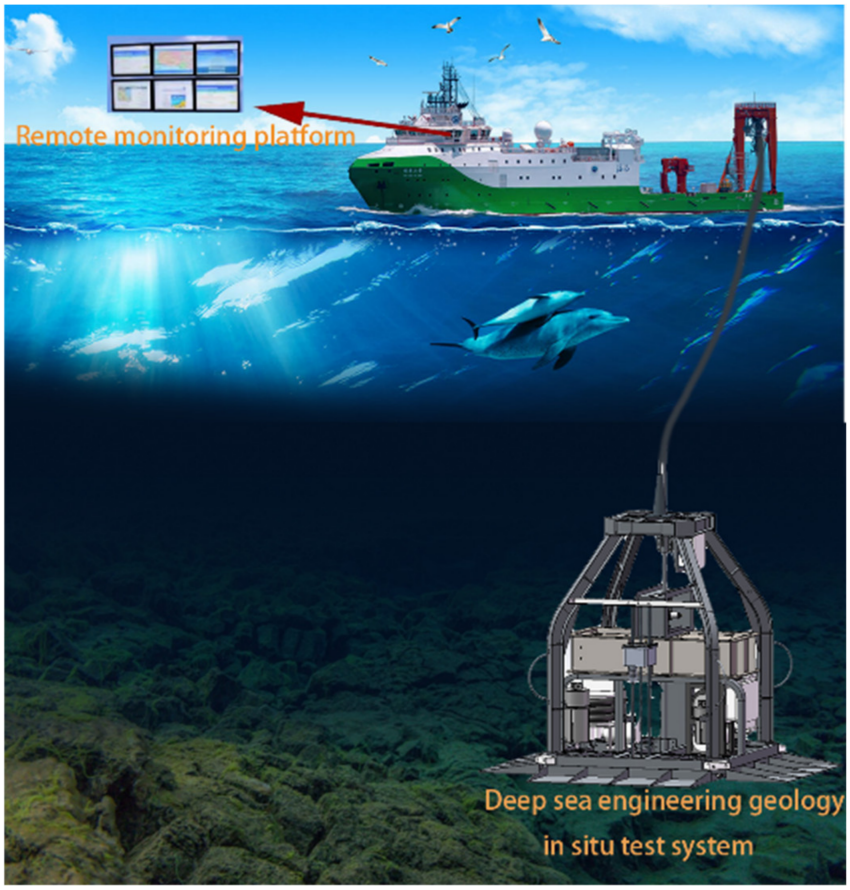


Figure 2. Schematic of the deep-sea engineering geology in situ test system in the offshore sea. Note this figure is not to scale.

The deep-sea engineering geology in situ test device adopts a frame structure, which is mainly divided into upper and lower layers. As shown in Figure 3, the photoelectric

composite umbilical cable on top of the device is mainly used for communication, power supply and load bearing. The upper layer is the penetration system, including the probe rod, penetration module and velocity measurement module of the digital CPTu and cross-shear device. The lower layer is the data acquisition and control system, including an altimeter, a depth meter, a tilt attitude measurement sensor, a photoelectric separation box, a transformer compartment, a low-voltage connection box, a high-voltage connection box and a control electronics compartment. Apron boards are installed at the bottom of the device to reduce the subsidence of the whole device in the deep-sea soft soil layer. The device on the upper and lower levels is described in detail below.

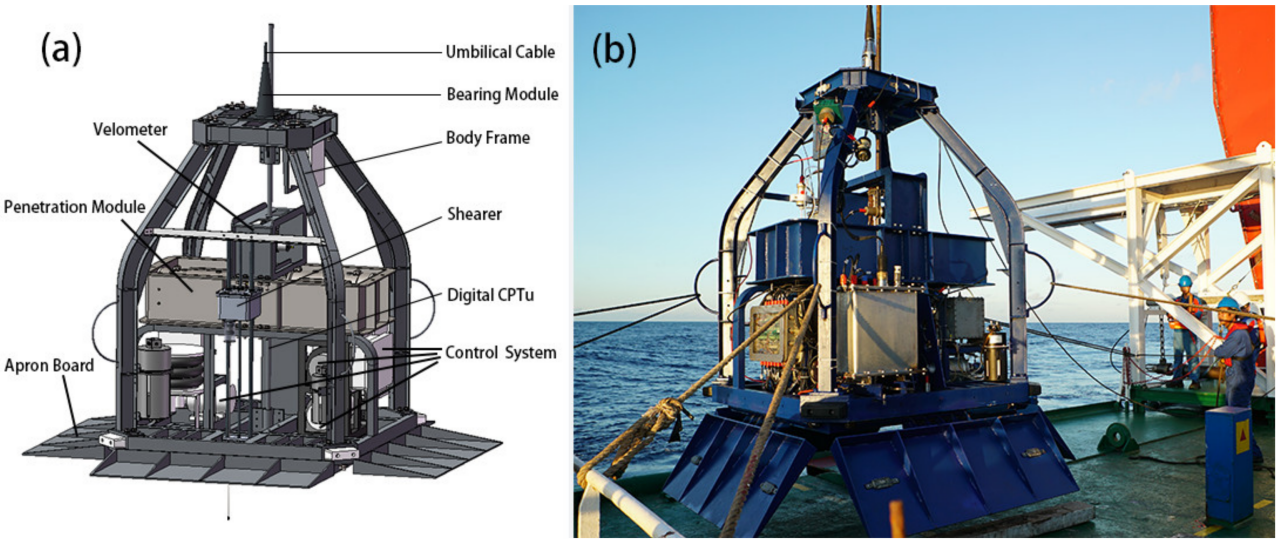


Figure 3. The deep-sea engineering geology in situ test device (**a**) Design schematic of the deep-sea engineering geology in situ test device, (**b**) Photo of the deep-sea engineering geology in situ test device.

2.1. Design of Digital CPTu

From the perspective of a mechanical structure, the probe of the digital CPTu is mainly composed of four parts from head to tail: the sensor cabin, the compensation cabin, the electronic cabin and the connecting joint, as shown in Figure 4.

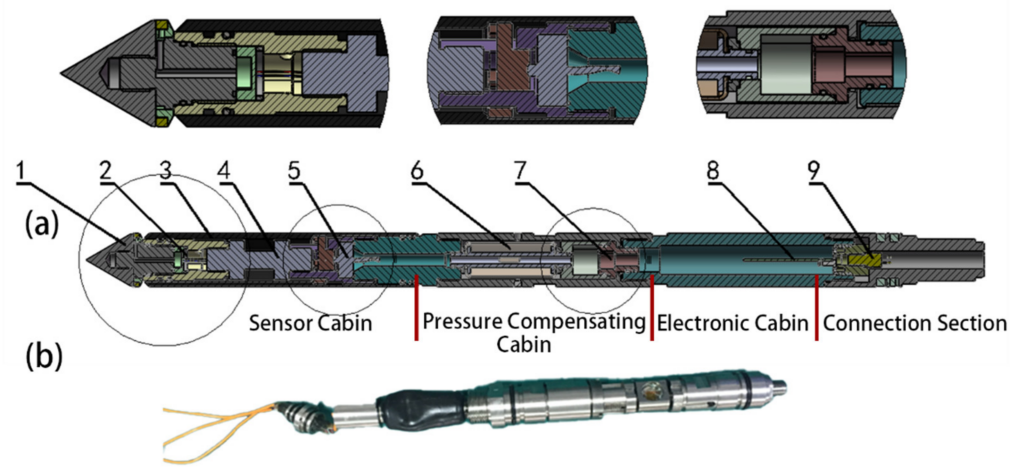


Figure 4. Digital CPTu probe (**a**) design schematic, (**b**) photograph, (1) cone, (2) pore pressure sensor, (3) friction sleeve, (4) cone resistance sensor, (5) sleeve friction sensor, (6) pressure-compensated oil capsule, (7) penetration piece A, (8) PCB board, (9) penetration piece.

The sensor cabin is the core of the digital CPTu probe, equipped with sensors for monitoring cone resistance, sleeve friction and pore pressure and their force transfer mechanisms. The force transfer mechanisms contain force elements and force transfer elements [35]. The cone head is the force element of the cone resistance, and it passes cone resistance to the cone tip resistance elastic element, the triangle claw and the electronic cabin in turn. The friction sleeve is the force element of the sleeve friction, and the sleeve friction data are transferred to the elastic element of sleeve friction and the electronic cabin through the friction sleeve successively. The pore pressure acts on the insulating oil inside the cone head through the permeable-stone ring assembled at the cone tip and is transmitted to the sensor. The dimensions of the sensor cabin are shown in Table 1.

Table 1. Dimensions of the sensor cabin.

Cone Bottom Cross-Sectional Area (cm^2)	Cone Bottom Diameter /tolerance (mm)	Cone Angle (°)	Friction Sleeve Superficial Area (cm^2)	Friction Sleeve Length (mm)
10	35.7/± 0.18	60/± 0.5	200	179/± 0.90

The compensation chamber is located in the middle of the digital CPTu probe and contains an oil capsule. The front of the capsule is connected to the sensor and is filled with insulating oil to provide pressure compensation and reduce the impact of external ultra-high hydrostatic pressure on test data. The rear of the oil capsule is isolated from the electronic compartment by penetration piece A, which can withstand ultra-high hydrostatic pressure. The oil capsule is made of butadiene rubber that has a soft texture and is easily deformed. The chemical properties of this rubber are very stable, and it has excellent oil and corrosion resistance. In the deep sea, the volume deformation of insulating oil occurs, and the oil capsule deforms under high pressure. Due to the smaller volume of the oil capsule, there is no internal force, except a small internal tension, when it is in a relaxed state.

The internal volume of the capsule, $V_{oil\ capsule}$, is given using the bulk modulus, K, of the oil filling the cavity in the CPTu cabin. The bulk modulus of liquid during compression at pressure P is expressed as follows:

$$K = \frac{P \cdot V_{total}}{\Delta V_{Total}} \tag{1}$$

where V_{total} is the total volume of liquid and ΔV_{Total} is the change in V_{total} during compression. In the CPTu cabin, V_{total} is expressed by the following equation:

$$V_{total} = V_{oil\ capsule} + V_{probe} \tag{2}$$

where V_{probe} is the internal volume of the probe not including the oil capsule. The ratio of the charge, η, in $V_{oil\ capsule}$ during compression, ΔV_{Total} to $V_{oil\ capsule}$, before compression is expressed as follows:

$$\eta = -\frac{\Delta V_{Total}}{V_{oil\ capsule}} \tag{3}$$

If V_{probe} is constant during compression, ΔV_{Total} in Equation (3) can be replaced by ΔV_{Total}, and $\Delta V_{oil\ capsule}$ is given by the following equation:

$$V_{oil\ capsule} = \frac{P \cdot V_{Probe}}{K \cdot \eta - P} \tag{4}$$

The electronic cabin is equipped with a signal acquisition and processing circuit board, which mainly realizes the "digital" function of conditioning the original test signal of each sensor and converting it into a digital signal and uploading it to the upper computer. The front perforator A isolates the high-pressure insulating oil inside the probe and the rear perforator B isolates the high-pressure seawater outside, creating a safe and dry

working environment for the circuit board and providing electrical connection access. The connection joint connects the main part of the probe and the probe rod to effectively and accurately transfer the penetration power generated by the penetration device to the probe. The digital CPTu has three models. All of them have the same shape but different parameters. The specifications of digital CPTu are shown in Table 2, where FS represents full scale.

Table 2. Specifications of digital CPTu (At 70 MPa hydrostatic pressure).

Model Num	I	II	III	Non-Linear Error	Repeatability Error	Hysteresis Error
Cone Resident (MPa/FS)	10	5	2	5%	5%	5%
Sleeve Friction (KPa/Fs)	100	50	25	5%	5%	5%
Pore Pressure (MPa/FS)	1	1	1	5%	5%	5%

The penetration module of the digital CPTu is shown in Figure 5. Its function is to stably and uniformly embed the digital CPTu in the soft soil layer of the seabed. The penetration module is composed of two sets of reducers, two friction wheels and a hydraulic unit. A reducer consists of a motor, a planetary gear, an output shaft with a small tooth difference and other units. The penetration module adjusts the position of the movable reduction gear by changing the hydraulic cylinder's variation to allow the two friction wheels to clamp onto the digital CPTu. The power of the reducer is transmitted by the motor. After passing through the planetary gear and the gear with a smaller tooth difference, the torque is transferred to the output shaft, and the friction wheel is rotated to realize the insertion and removal of the digital CPTu. The function of the oil capsule is to balance the internal and external pressure of the penetration module.

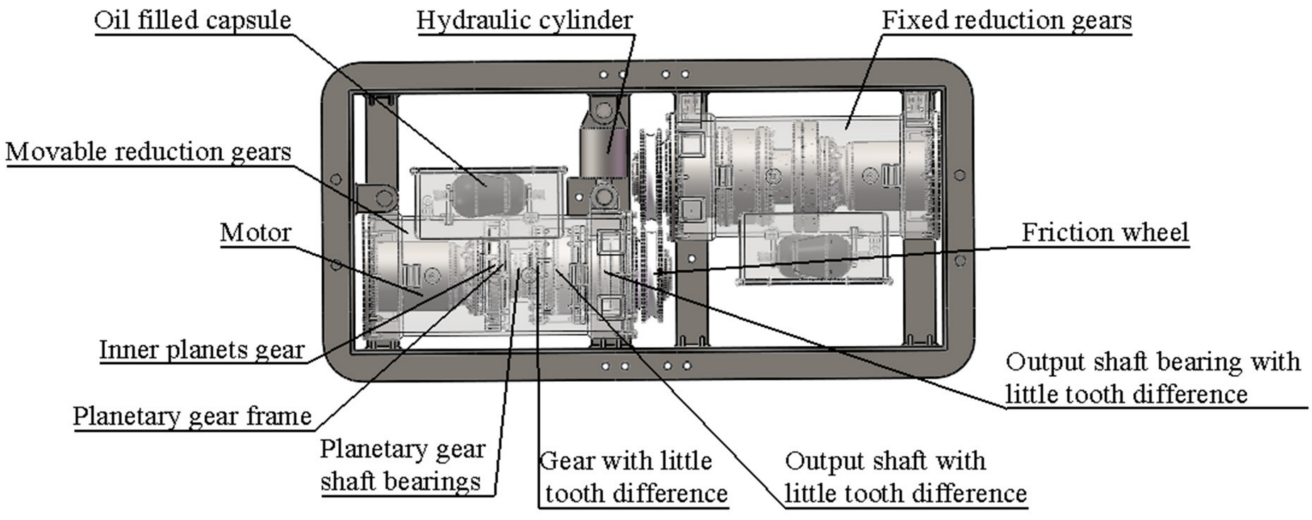


Figure 5. Design schematic of penetration module for the digital CPTu.

2.2. Design of Cross-Shear Device

As shown in Figure 6, the cross-shear device consists of a smooth rod, a lead rod, a penetration module, a shear drive module, a torque sensor and a cross-shear plate. Through the penetration module, the cross-shear device is pushed downward in the direction of the smooth rod and lead rod. When the cross-shear plate reaches a predetermined depth, the shear drive module is controlled to make the cross-shear plate rotate at an even speed in

the soil. The mechanical parameters and specifications of the cross-shear device are shown in Tables 3 and 4, where FS stands for full scale.

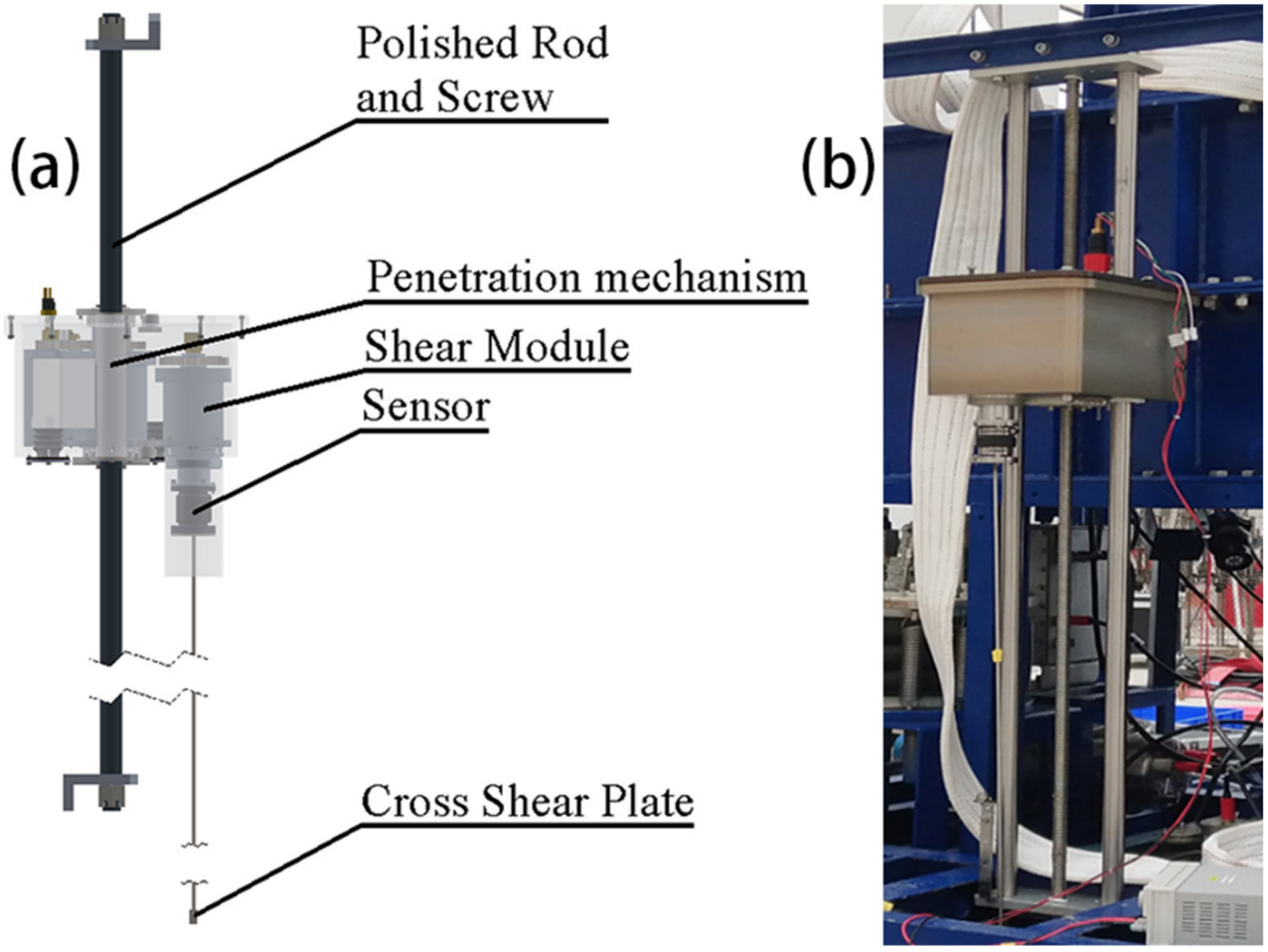


Figure 6. (**a**) Design schematic of cross-shear device, (**b**) photo of cross-shear device.

Table 3. Specifications of shear sensor.

Range (N/m)	Non-Linear Error /FS	Repeatability Error/FS	Hysteresis Error /FS
6	≤0.5%	≤0.5%	≤0.5%
9	≤0.5%	≤0.5%	≤0.5%
12	≤0.5%	≤0.5%	≤0.5%

Table 4. Design parameters of mechanical components of cross-shear plate.

Width (mm)	Height (mm)	Thickness (mm)	Rod Diameter (mm)	Rod Length (mm)
30	60	2	13	1060

2.3. Design of Control System

In order to enhance the scalability of the hardware system, we adopted a modular design for the hardware of the control system. It is easy to repair when modules fail and to expand when new sensors need to be added. As shown in Figure 7, the control system can be divided into two parts: the surface system and the underwater system. The surface system is mainly composed of software, which is primarily responsible for command

sending and receiving, data transmission, storage and logic algorithm processing, and controlling the underwater system through a serial port. The underwater system is mainly responsible for the power management, task scheduling and data transmission of the system. The control system can control the digital CPTu, cross-shear device, altimeter, depth meter and other data acquisition methods and switch devices on and off through the independent communication interface and power interface. It can also control the motor to achieve stable continuous penetration and extraction of the rod. All hardware of the subsea system is packaged according to its function in the above-mentioned pressure-bearing cabins, which are connected to each other through watertight joints and oil-filled cables.

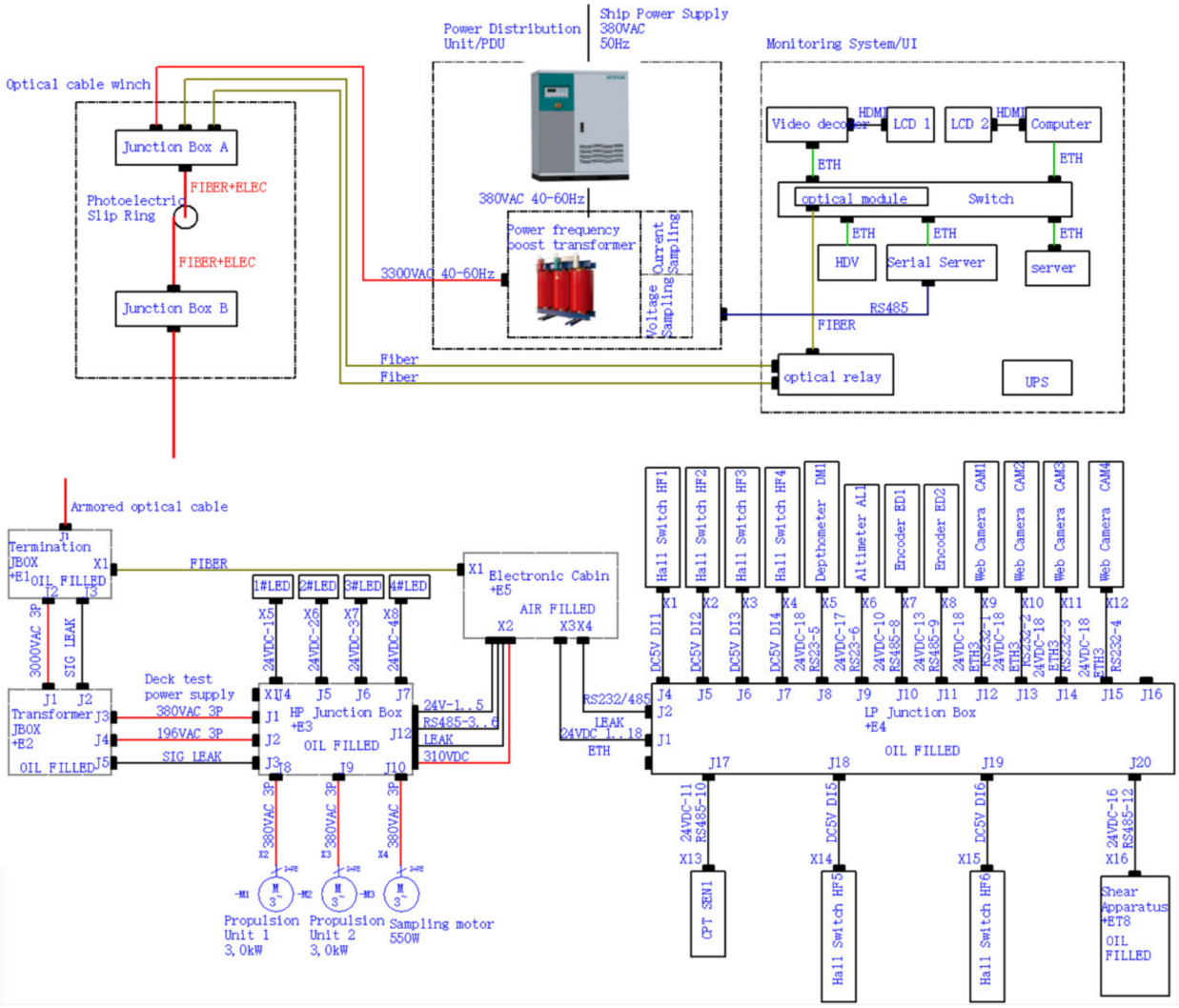


Figure 7. General control structure diagram.

3. Land Experiment

In order to verify the reliability and accuracy of the deep-sea engineering geology in situ test system, we conducted land experiments, and this experience can be used as the basis for deep-sea experiments. During the land experiment for the digital CPTu, due to the limitations of the site, we dug a well with a depth of about 3 m and diameter of 90 cm, and built a hollow cement sleeve with an inner diameter of about 70 cm to prevent the collapse of the well wall. We firstly laid down a 0.5 m original soil layer, and then an artificial clay layer with a thickness of about 2 m in the cement sleeve, and finally laid down a 0.5 m original soil layer, to form a soil layer structure of "natural soil layer (0.5 m)—artificial clay layer (2 m)—natural soil layer (0.5 m)" from top to bottom. Artificial clay is a clay-like

mixed material made by mixing inorganic bentonite (mainly composed of montmorillonite, silica and alumina) and water in a certain proportion. Artificial clay has low penetration resistance and friction, and good water retention.

We used a matching probe and three independently designed digital CPTus for the land experiments, as shown in Figure 8. The specifications and mechanical parameters of the matching probe are shown in Tables 5 and 6. The matching probe had no digitization function, and its sensor output is analog signals. Therefore, the matching probe was modified: an extra cabin was connected to the tail of the matching probe, and a signal acquisition and processing circuit was placed inside, which converts the sensor signal into a digital signal and uploads it. The digital CPTu was applied to the extremely thin and soft seabed soil layer. There was little resistance, and the corresponding force range was not too large; otherwise, the accuracy would have been affected. However, the range selected for the matching probe was much larger than the range of the digital CPTu. This is because the matching probe is a commercial land probe, and the range of cone tip resistance is generally several tons to tens of tons, and three tons is the minimum range of probes available for purchase.

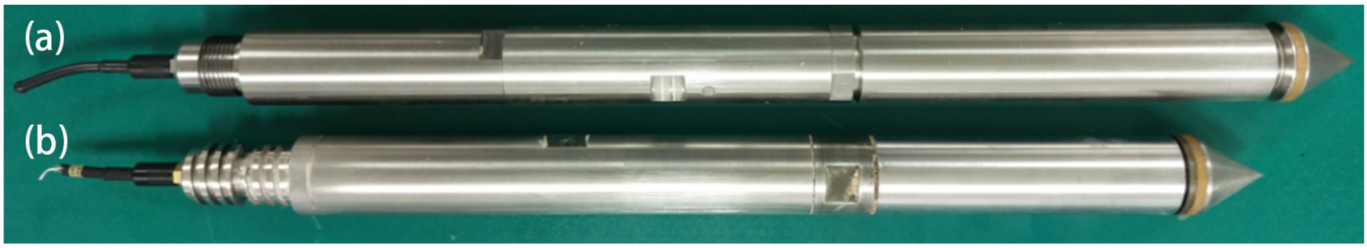


Figure 8. (**a**) Independently designed digital CPTu, (**b**) matching probe.

Table 5. Specifications of the matching probe.

Cone Resistance (MPa)	Sleeve Friction (KPa)	Pore Pressure (MPa)
30	375	1

Table 6. Design parameters of the mechanical parts of the matching probe.

Length (mm)	Sectional Area (cm^2)	External Diameter (mm)	Taper Angle (°)
650	10	35.68	60

Figure 9 shows, from left to right, the curve of cone resistance, sleeve friction and pore pressure at a 3 m penetration depth of the matching probe and the three digital CPTu devices in the land test. The tests were carried out in the following sequence: matching probe, probe I, probe II and probe III. From the curve analysis, the repeatability of cone resistance, sleeve friction and pore pressure measured by the matching probe was better than that of the digital CPTu. In terms of repeatability, the performance of digital CPTu I, II and III decreased successively. However, the smaller the full scale of the digital CPTu probe, the higher the resolution and the more detail it reflected. In the curve of cone resistance and depth, the digital CPTu should have showed a small peak at the depth of 0.5 m, but with the increase in the number of tests, the height of the peak continuously decreased and moved to the left, and this also occurred at the depth of 3 m. The other two curves also demonstrated that the digital peak value and position changed with the increase in test times at the boundary of the soil layer.

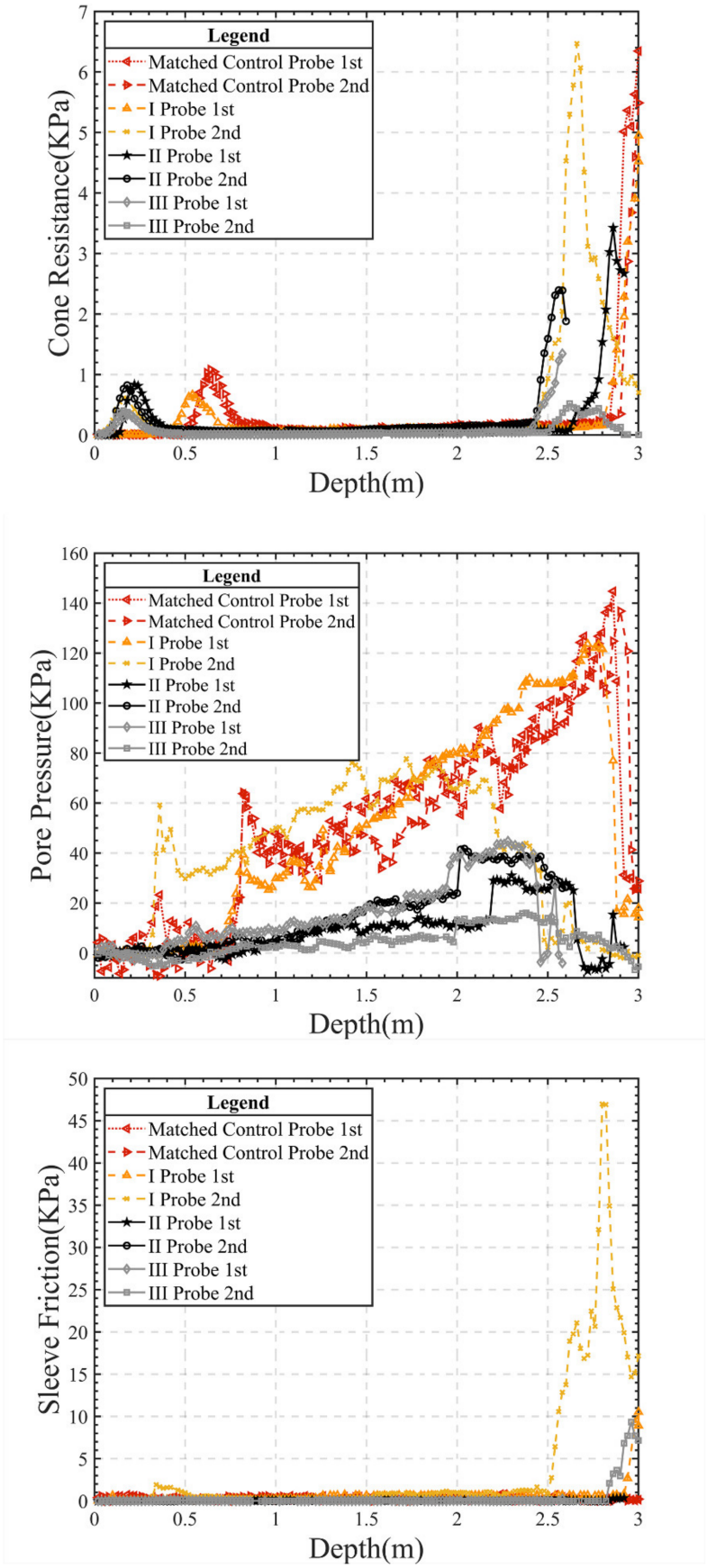


Figure 9. Land experiment: cone resistance curve, sleeve friction curve and pore pressure curve with respect to depth.

The artificial clay mentioned above was used as the shear sample soil when we tested the cross-shear device. Three sampling times were examined in this test. The sampling interval was 80 mm, the rotation angle was 90°, the descent speed was 0.5 mm/s, and the transmission speed was 1°/s. The results are shown in Figure 10. All three curves reached the peak value of shear resistance when the shear angle was about 6°. Within the interval of 0~6°, the three curves had the same upward trend, but within the range of 6~90°, the first curve had the steepest downward trend. The downward trend of the second curve was relatively slow, but there were small spikes in the second half of the curve. The third curve was the flattest and smoothest of the three.

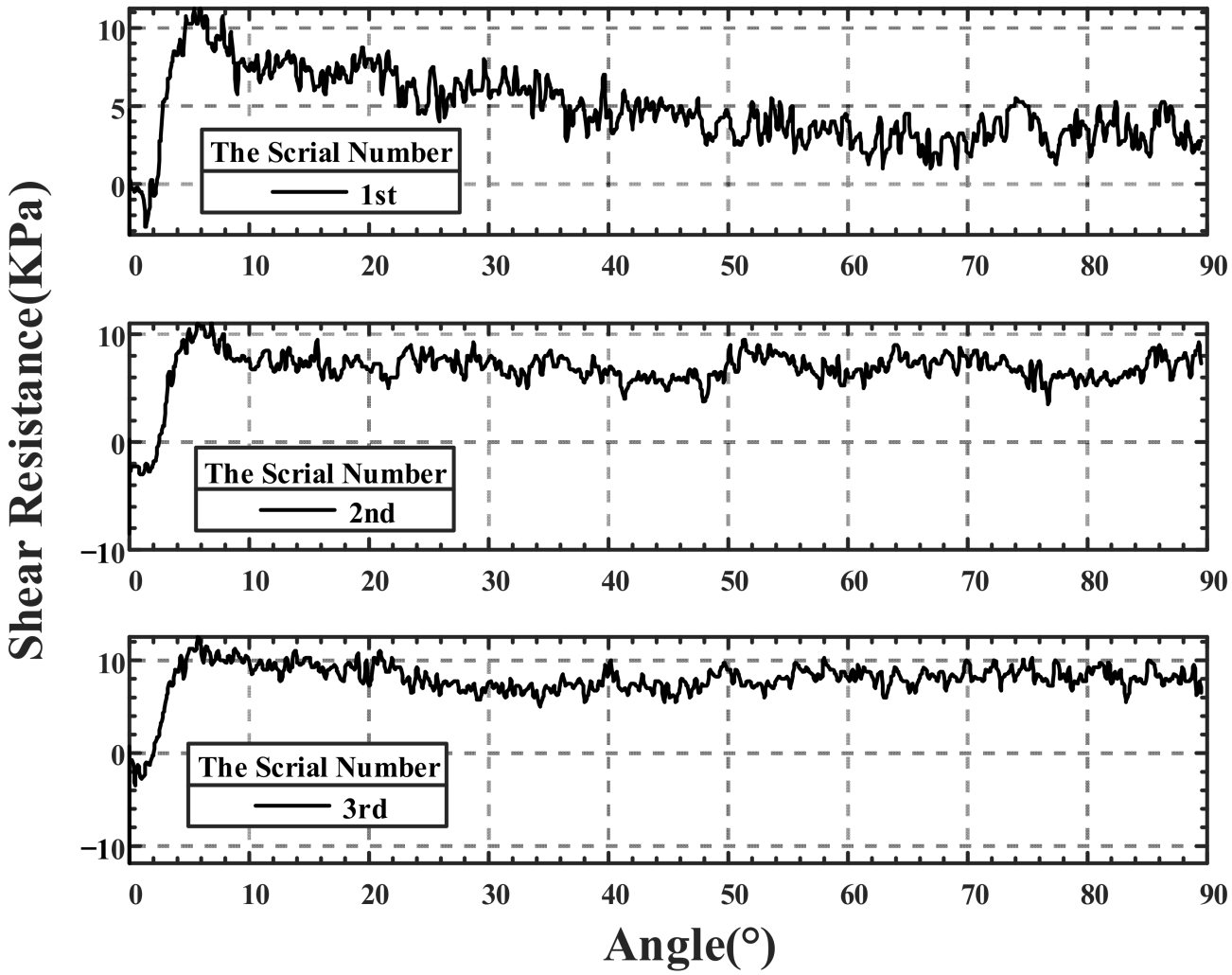


Figure 10. Land experiment: shear resistance curve with respect to angle.

After a comprehensive analysis of the land test for the digital CPTu and the matching probe and the cross shear, we determined the following reasons for the decrease in the local peak value of the curve of the digital CPTu, the shift in position to the left and the local difference in the descending region of the curve of the cross shear: The small land test area decreased the penetration point spacing of each test. The further the depth at which the probe conducted data acquisition and cross shear measurement, the more affected the penetration tests. However, the basic trend of the curve reflects the characteristics of the ideal stratum, such as the interface between the upper natural soil layer and the middle artificial clay, and the interface between the middle artificial clay and the lower natural soil. Therefore, the independently designed digital CPTu and cross-shear devices all fulfilled the purpose of the test.

4. Sea Trials

4.1. Trail Site

According to the test requirements of the deep-sea engineering geology in situ test system, we selected three test areas, as shown in Figure 11, A, B and C, whose depths were 100 m, 1000 m and 3000 m, respectively. In this sea trial, the digital CPTu device obtained datasets from five stations, and the cross-shear device obtained datasets from three stations.

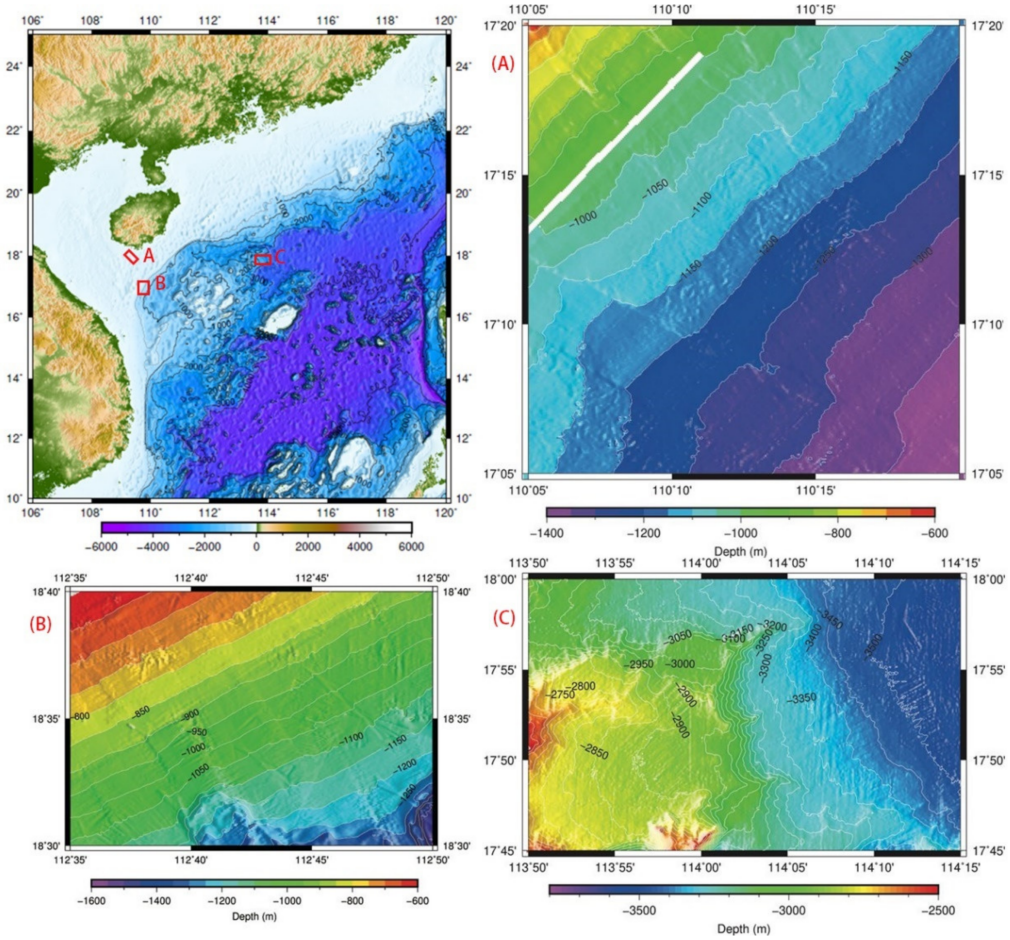


Figure 11. Location of in situ test. Test area A is near Sanya Wharf, and its depth is 100 m; test area B is located at E 110°05′~110°20′, N 17°05′~17°20′, and its depth is 1000 m; test area C is located at E113°50′~114°, N 17°45′~18°, and its depth is 3000 m.

4.2. Data Processing

The data obtained from sites 2 and 3 in region C are taken as an example for analysis. Cone resistance, sleeve friction and pore pressure data were obtained for a depth of approximately 6.5 m, and cross-shear data were at a depth of 1 m. A digital CPTu II and the cross-shear sensor measuring range of 9 N/m was used in the test.

The original data obtained by the digital CPTu contained noise, which made the curve of cone resistance, sleeve friction and pore pressure jagged and irregular with local spikes interspersed and spaced at short intervals, as shown in Figure 12. Therefore, before the soil classification, we used a wavelet denoising method to optimize the data. The processed data waveform was relatively smooth, eliminating the fuzzy fluctuation phenomenon of the original data, and retaining the overall trend and details of the original data, as shown in Figure 13.

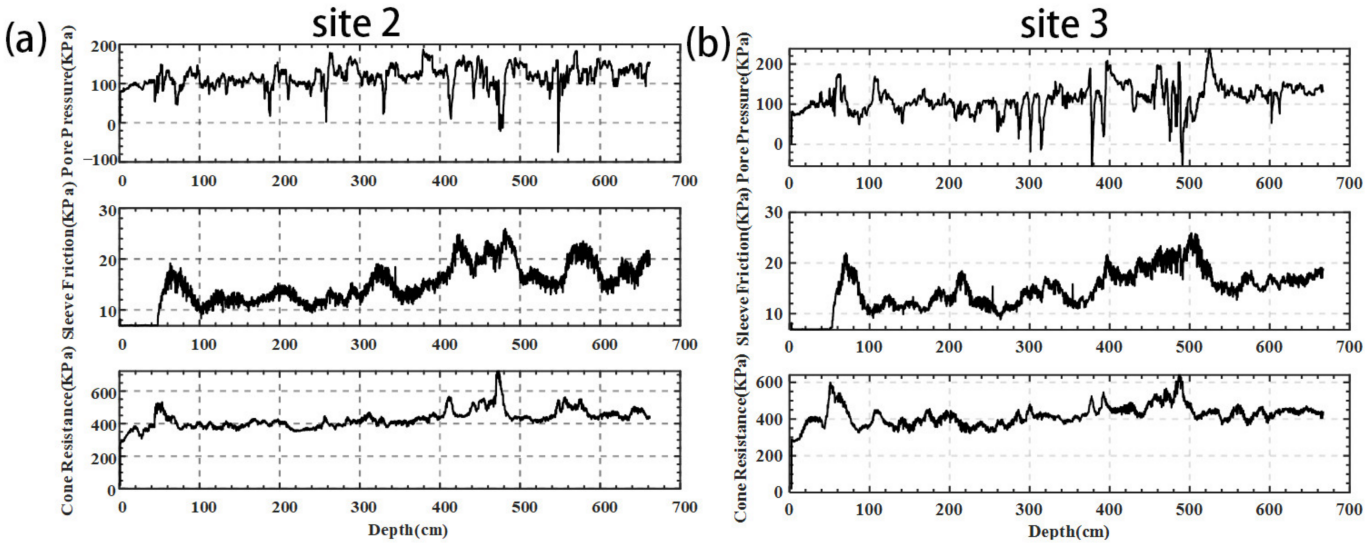


Figure 12. Raw data of digital CPTu: (**a**) site 2 and (**b**) site 3.

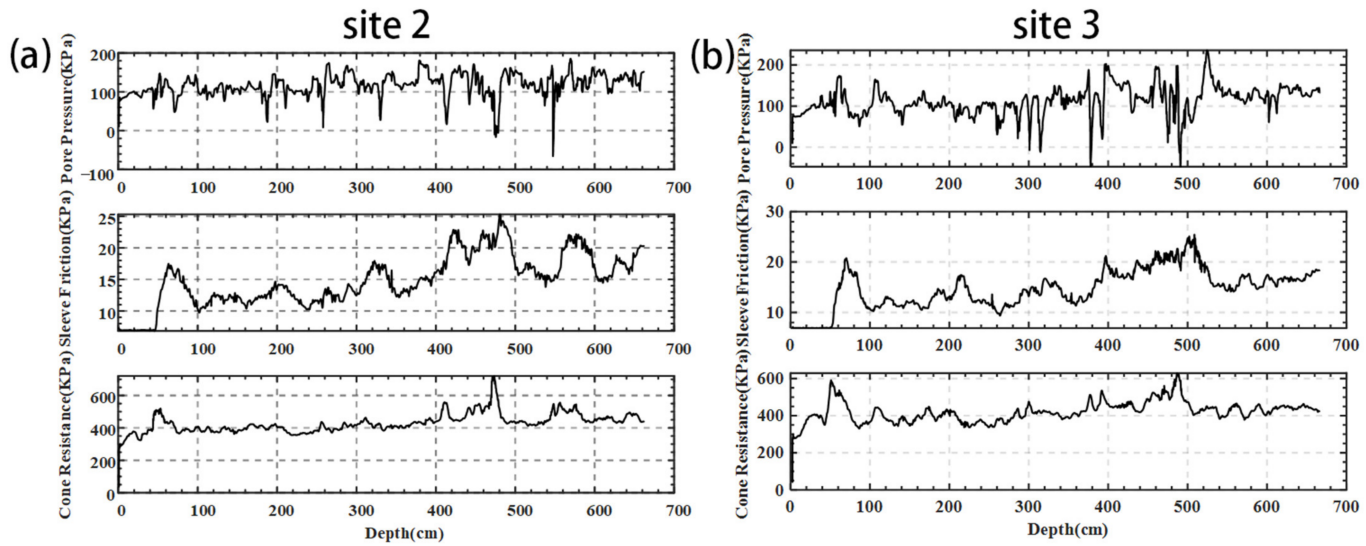


Figure 13. Optimized digital CPTu data: (**a**) site 2 and (**b**) site 3.

In soil classification, the Robertson soil classification map [38,39] and Eslami–Fellenius soil classification map [40,41] are commonly used internationally. Although the Robertson soil classification map can be used to accurately identify the excavated category, it requires a bulk density value to accurately reflect the overlying earth pressure. Without detailed laboratory tests, the map is too complicated and difficult to use for practical engineering purposes. When using the Eslami–Fellenius soil classification map, the effective cone resistance is used instead of the original cone resistance value and the correct value of cone resistance, which can prevent data distortion. Moreover, the Eslami–Fellenius soil classification map only needs cone resistance, sleeve friction and pore pressure to accurately determine the soil category. Therefore, the Eslami–Fellenius soil classification map was used in this study to distinguish the soil properties of the data, as shown in Figure 14.

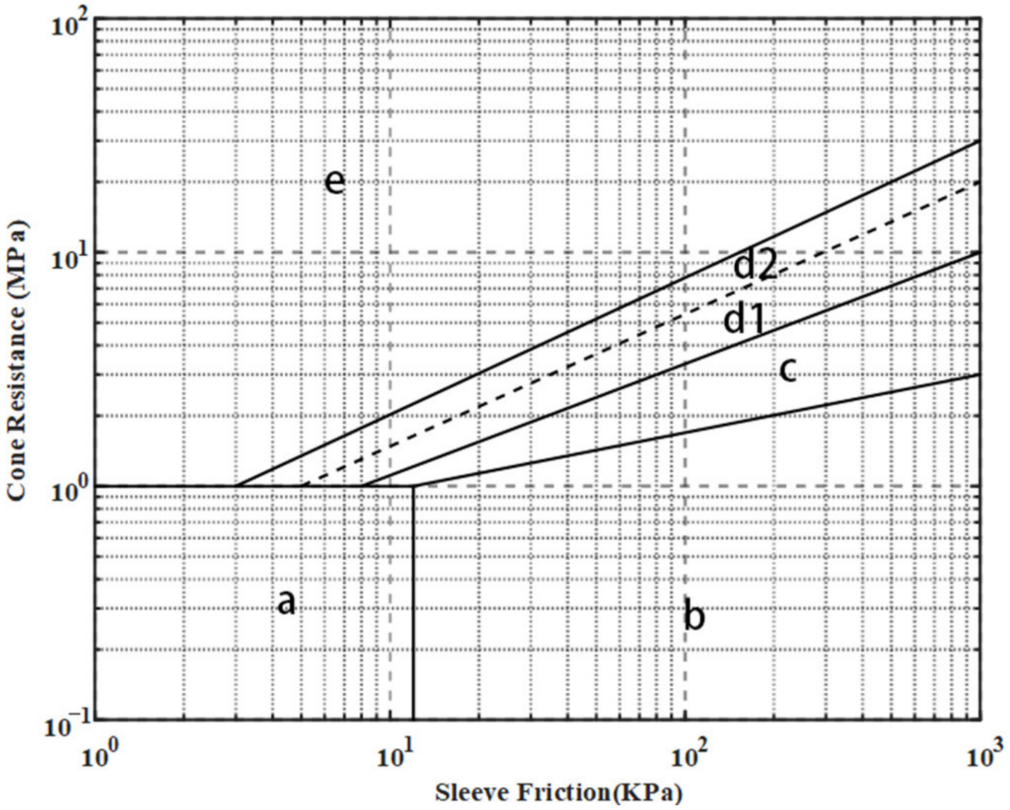


Figure 14. Eslami–Fellenius soil classification figure [24]: (**a**) very soft clays, or sensitive or collapsible soils, (**b**) clay and/or silt, (**c**) clayey silt and/or silty clay, (**d1**) sandy silt, (**d2**) sandy sand and (**e**) sand to sandy gravel.

The results of data discrimination using the Eslami–Fellenius soil classification map are shown in Figure 15. According to the figure, the soil layers of this site are concentrated in two regions, a and b. According to these datasets, cone resistance does not exceed 1 MPa in these two sites; hence, the main factor affecting the classification of soil layer at this site is sleeve friction, as shown in Figure 16. From the overall trend of the curve, it can be seen that with the increase in penetration depth, the soil composition changed from very soft clays, or sensitive or collapsible soils in area A, to very soft clays, or sensitive or collapsible soils, and clay and/or silt in area B, and finally to clay and/or silt in area C. The penetration depths of area A, B and C were 0–52 cm, 56–284 cm and 284–662 cm, as shown in Figure 16a, and the penetration depths of area A, B and C were 0–56 cm, 56–360 cm and 360–667 cm, respectively, as shown in Figure 16b. We speculate that the main factor affecting soil property discrimination of this site is soil moisture content. Region A is critical for seafloor liquid–solid exchange and had the largest moisture content, so it was determined to be collapsible clay/clay silt, while region C had the least relative water content, so it was all clay/clay silt. Meanwhile, region B was the transition region between A and C. Due to the nature and distribution of the soil, the distribution of water content was not uniform, resulting in the alternating occurrence of collapsed clay/clay silt and clay/clay silt.

Cross-shear data are shown in Figure 17. For site 3, subgraph a is the shear resistance curve obtained using the cross-shear plate in the same angle range at different depths. Subgraph b is the curve drawn by interpolating the maximum value of the curve at different depths in subgraph a. It can be seen from subgraph b and subgraph d that the max shear resistance increased with increasing depth in the region of 0–66 cm, reached a peak at about 66 cm depth, and then decreased with depth. Therefore, in engineering applications, it can

be considered that the shear resistance decreases and the efficiency decreases when the depth exceeds 66 cm.

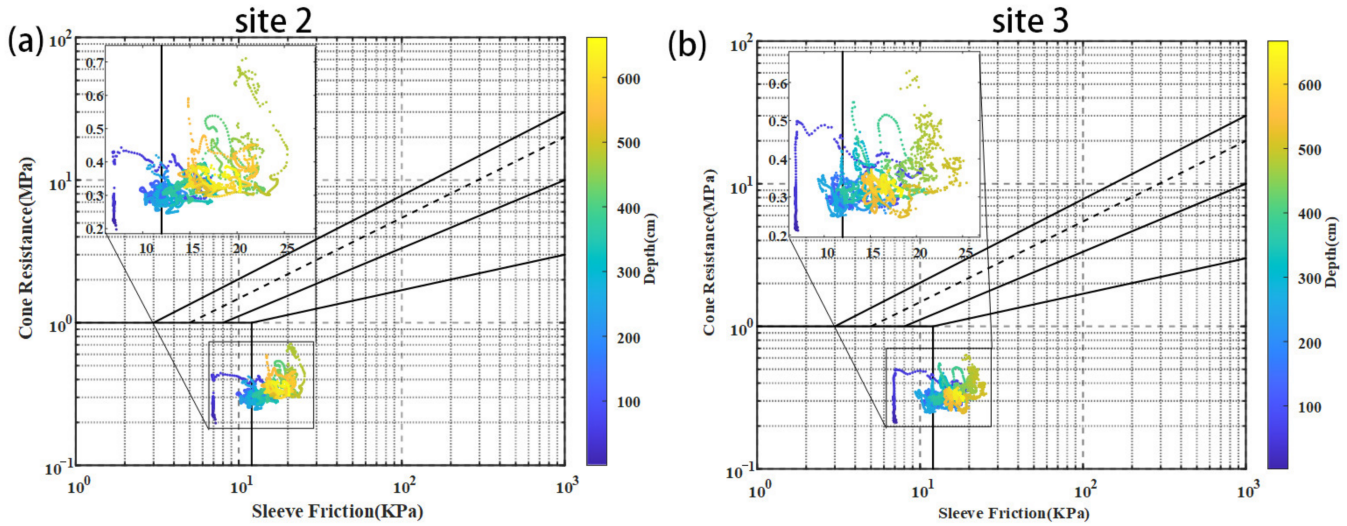


Figure 15. Image of soil classification results: (**a**) site 2 and (**b**) site 3.

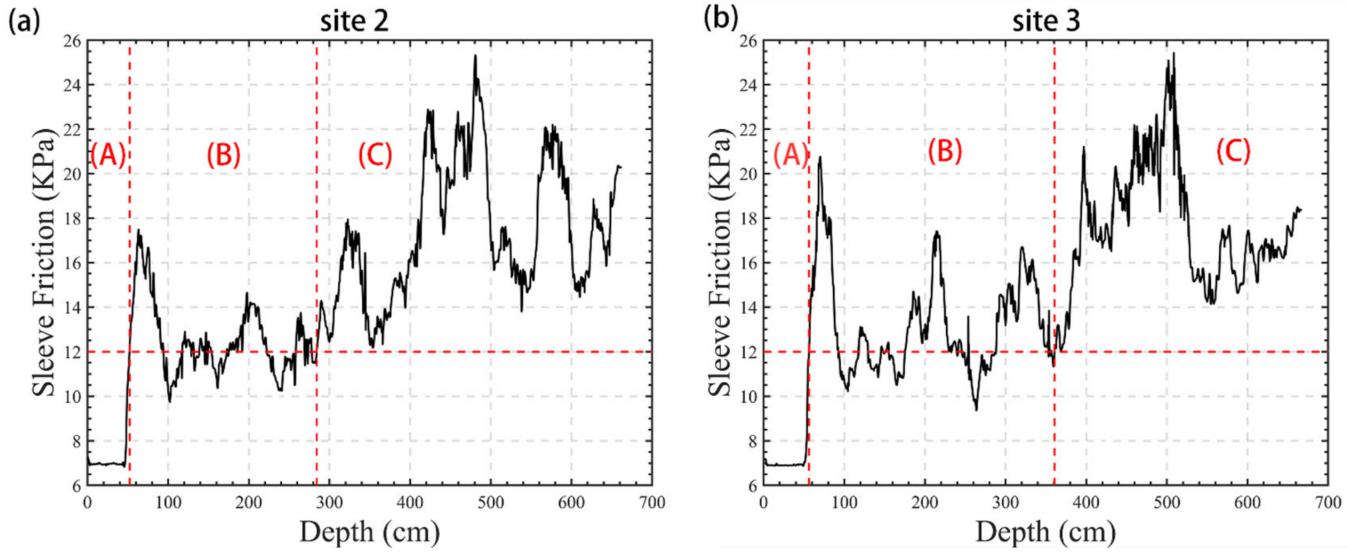


Figure 16. Image of the relationship between sleeve friction and depth: (**a**) site 2 and (**b**) site 3. A is the region of "Very Soft Clays, or Sensitive or Collapsible Soils"; C is the region of "Clay and/or Silt"; B is the region alternating between A and C.

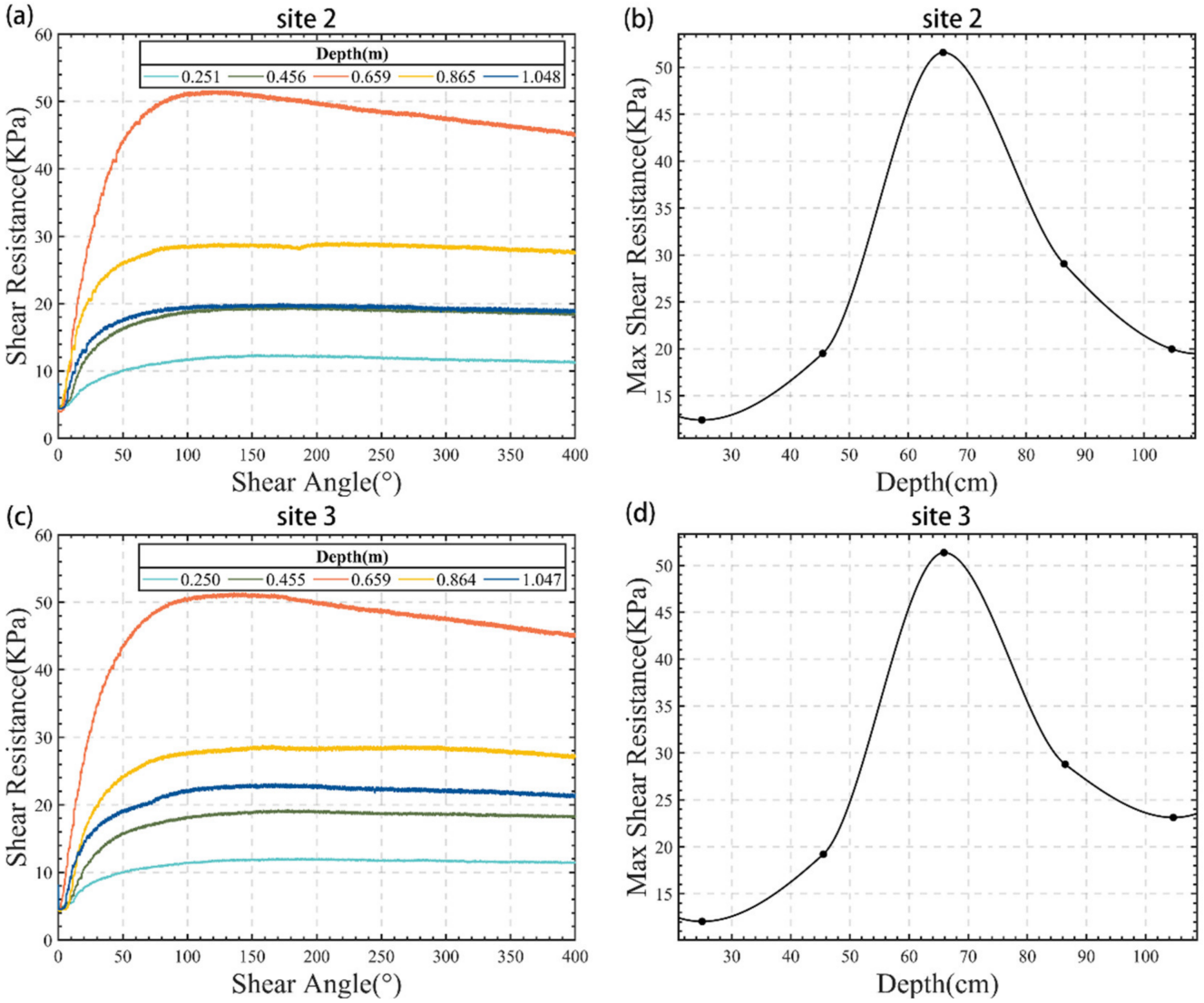


Figure 17. (**a**) Shear resistance curve in site 2, (**b**) curve of max shear pressure with depth in site 2, (**c**) shear resistance curve in site 3, (**d**) curve of max shear pressure with depth in site 3.

5. Conclusions

In this study, we developed a deep-sea engineering geology in situ test system for detecting the mechanical properties of seafloor sediments. It was mainly composed of a penetration system and a measurement and control system. We conducted land tests on the digital CPTu and cross-shear device of the deep-sea engineering geology in situ test device, and verified their reliability and accuracy. Subsequently, we collected data from five sites in three regions of the South China Sea. Analysis of the collected data shows that at a 3000 m water depth, the seafloor surface sediment, which is critical for seafloor liquid–solid exchange, transitions from collapsing clay/clay silt to clay/clay silt with penetration depth. Meanwhile, the obtained values of cone resistance, sleeve friction, pore pressure and cross-shear resistance provide mechanical data support for the application of deep-sea engineering devices in this area.

Author Contributions: Conceptualization, M.C.; methodology, K.Z.; writing—original draft preparation, K.Z.; writing—review and editing, M.C., K.Z., C.X., W.C., J.Z., W.O. and C.Y.; supervision, M.C.; project administration, M.C.; All authors have read and agreed to the published version of the manuscript.

Funding: This research was supported by the Strategic Priority Research Program of Chinese Academy of Sciences, "Deep-sea and Hadal Intelligent Technology and Seafloor Science Laboratory", Grant No. XDA22040301.

Data Availability Statement: Not applicable.

Acknowledgments: We sincerely thank the editors and the anonymous reviewers for their constructive comments. Sincere thanks go to Chao Xie, Wei Chen, Jingrong Zheng, Wen Ou and Chunliang Yu for their help in carrying out the in situ and laboratory experiments.

Conflicts of Interest: The authors declare no conflict of interest.

References

1. Wang, X.M.; Sun, Z.S. Status and exploitation prospect of world- wide marine mineral resources. *World Nonferrous Met.* **2010**, *6*, 21–25. [CrossRef]
2. Qi, H.E.; Wang, P. Current Situation and Prospect of Deep Sea Energy Development. *Ocean. Dev. Manag.* **2017**, *34*, 66–71.
3. Kato, Y.; Fujinaga, K.; Nakamura, K.; Takaya, Y.; Kitamura, K.; Ohta, J.; Toda, R.; Nakashima, T.; Iwamori, H. Deep-sea mud in the Pacific Ocean as a potential resource for rare-earth elements. *Nat. Geoence* **2011**, *4*, 535–539. [CrossRef]
4. Petersen, S.; Krätschell, A.; Augustin, N.; Jamieson, J.; Hein, J.R.; Hannington, M.D. News from the seabed—Geological characteristics and resource potential of deep-sea mineral resources. *Mar. Policy* **2016**, *70*, 175–187. [CrossRef]
5. Schulte, E.; Handschuh, R.; Schwarz, W. Transferability of Soil Mechanical Parameters to Traction Potential Calculation of a Tracked Vehicle. In Proceedings of the 5th ISOPE Ocean Mining Symposium, Tsukuba, Japan, 15–19 September 2003.
6. Barnes, C.R.; Tunnicliffe, V. Building the World's First Multi-node Cabled Ocean Observatories (NEPTUNE Canada and VENUS, Canada): Science, Realities, Challenges and Opportunities. In Proceedings of the OCEANS 2008—MTS/IEEE Kobe Techno-Ocean, Kobe, Japan, 8–11 April 2008; pp. 1–8. [CrossRef]
7. Ehlers, C.J.; Chen, J.; Roberts, H.H.; Lee, Y.C. The Origin of Near-Seafloor "Crust Zones" in Deepwater. Available online: https://digitalcommons.lsu.edu/geo_pubs/1624/ (accessed on 23 January 2023).
8. Liangqing, S. Geotechnical properties of oceanic polymetallic nodule sediments. *Acta Oceanol. Sin.* **1999**, *21*, 47–54.
9. Wu, H.Y.; Chen, X.M.; Gao, Y.Q.; He, J.S.; Liu, S.J. In-Situ shearing strength and penetration resistance testing of soft seabed sediments in western mining area. *J. Cent. South Univ. Sci. Technol.* **2010**, *41*, 1801–1806.
10. Wang, C.; Yanjiang, Y.U.; Kou, B. Summary of Marine In-Situ Testing Methods. *Ocean Dev. Manag.* **2017**, *34*, 81–86.
11. Chu, Y.; Cai, G.J.; Liu, S.Y. Study on Liquefaction Estimation Method Based on State Parameters of CPTU in Situ Measurement. *China Earthq. Eng. J.* **2014**, *36*, 905–910.
12. Tang, A. A guide to penetration testing. *Netw. Secur.* **2014**, *2014*, 8–11. [CrossRef]
13. Lu, F.C.; Qu, Y.D.; Liao, M.H. The Development Status and Applications of In Situ Cone Penetration Test Technology. *Ocean Technol.* **2004**, *23*, 32–36.
14. Chen, Q.; Shi, Y.H.; Pan, Y. Downhole technology for submarine CPT and its device development. *Ocean Eng.* **2007**, *25*, 73–76.
15. Sacchetto, M.; Trevisan, A.; Elmgren, K.; Melander, K. *CPTWD (Cone Penetration Test While Drilling) a New Method for Deep Geotechnical Surveys. Geotechnical and Geophysical Site Characterization, Vol. 1 and 2*; Millpress Science Publishers: Amsterdam, The Netherland, 2004.
16. Lunne, T. The CPT in offshore soil investigations—A historic perspective. *Proc. CPT* **2010**, *10*, 71–113.
17. Guo, S.Z.; Liu, R. Application of cone penetration test in offshore engineering. *Chin. J. Geotech. Eng.* **2015**, *37*, 207–211.
18. Zhang, H.; Jia, Y.; Liu, X.; Wei, Z.; Ji, C.; Jiao, X.; Zhu, C. Progress in In-Situ Measurement of Sediment Mechanical Properties for Full Ocean Depth. *Mar. Geol. Front.* **2019**, *35*, 1–9.
19. Bouwmeester, D.; Peuchen, J.; Van, D.; Sarata, B.; Willemse, C.; Van Baars, S.; Peelen, R. Offshore Technology Conference—Prediction of Breakout Forces for Deepwater Seafloor Objects. In Proceedings of the Offshore Technology Conference Offshore Technology Conference, Houston, TX, USA, 4 May 2009.
20. Qi, C.; Xing, X.; Shi, Y.; Pan, Y. The Status and Development of Offshore Cone Penetration Testing at Home and Abroad. *Geol. Res. South China Sea* **2009**, 8–89.
21. Fudong, J.; Yonggang, J.; Xiaolei, L. Development and Application of New Offshore CPT Equipment. *Coast. Eng.* **2016**, *35*, 1–9.
22. Shi-Min, L. *Research on the Mechanical Structures of CPT System on Seabed of Shallow Ocean Area*; Jilin University: Jilin, China, 2005.
23. Dao-Hong, Q. *Research on the Mechanical Structures of Tracked Carrier on CPT of Tidal Flat*; Jilin University: Jilin, China, 2005.
24. Jiang, Y.Y. *The Study of Cone Penetration Testing Methods and the Application in Offshore Engineering*; Tianjin University: Tianjin, China, 2011.
25. Ji, F.; Jia, Y.; Liu, X.; Guo, L.; Zhang, M.; Shan, H. In Situ Measurement of The Engineering Mechanical Properties of Seafloor Sediment. *Mar. Geol. Quat. Geol.* **2016**, *36*, 191–200.

26. Zhongde, G.; Xingsen, G.; Wei, Z.; Xing, W.; Xiaolei, L.; Jingbin, Z.; Jingxi, L.; Yonggang, J.; Tingkai, N. Multi-probe in-situ testing system and evaluation method for undrained shear strength of deep-sea shallow sediments. *J. Eng. Geol.* **2021**, *29*, 1949–1955.
27. Liu, Y.; Zhu, H.Z.; Chen, G.B.; Zheng, H.J.; Wang, C.G. Development and application of the PeneVector Down-hole System. In Proceedings of the 15th National Conference on Engineering Geophysical Prospecting and Geotechnical Engineering Testing, Xiamen, China, 8–10 November 2017; pp. 55–56.
28. Morgan, N.; Cathie, D. Tracked subsea trencher mobility and operation in soft clays. In Proceedings of the Sixteenth International Offshore and Polar Engineering Conference, Lisbon, Portugal, 1–6 July 2007. ISOPE-I-07-355.
29. Hong, S.; Kim, H.W.; Choi, J.S. Transient dynamic analysis of tracked vehicles on extremely soft cohesive soil. In Proceedings of the International Society of Offshore & Polar Engineers Pacific/Asia Offshore Mech Symp, Daejeon, Republic of Korea, 17 November 2002.
30. Dai, Y.; Liu, H.; Zhang, T.; Liu, S.J. Research on traction trafficability of seafloor tracked mining vehicle. *China Sci.* **2015**, *10*, 1203–1208.
31. Steiner, A.; Kopf, A.J.; Henry, P.; Stegmann, S.; Apprioual, R.; Pelleau, P. Cone penetration testing to assess slope stability in the 1979 Nice landslide area (Ligurian Margin, SE France)—ScienceDirect. *Mar. Geol.* **2015**, *369*, 162–181. [CrossRef]
32. Lunne, T. The Fourth James K. Mitchell Lecture: The CPT in offshore soil investigations—A historic perspective. *Geomech. Geoengin.* **2012**, *7*, 75–101. [CrossRef]
33. Sultan, N.; Voisset, M.; Marsset, T.; Vernant, A.M.; Cauquil, E.; Colliat, J.L.; Curinier, V. Detection of free gas and gas hydrate based on 3D seismic data and cone penetration testing: An example from the Nigerian Continental Slope. *Mar. Geol.* **2007**, *240*, 235–255. [CrossRef]
34. Boggess, R.; Robertson, P. CPT for Soft Sediments and Deepwater Investigations. In Proceedings of the Offshore Technology Conference, Houston, TX, USA, 2–5 May 2011. [CrossRef]
35. Jorat, M.E.; Kreiter, S.; Mörz, T.; Moon, V.; de Lange, W. Utilizing Cone Penetration Tests for Landslide Evaluation. In *Submarine Mass Movements and Their Consequences. Advances in Natural and Technological Hazards Research*; Springer: Cham, Switzerland, 2014; Volume 37.
36. Hawkins, R.A.; Markus, A. New Developments in Offshore Geotechnical Investigations. In Proceedings of the Offshore Site Investigation and Foundation Behaviour. Available online: https://onepetro.org/SUTOSIF/proceedings-abstract/OSIFB98/All-OSIFB98/SUT-OSIFB-98-259/3130 (accessed on 23 January 2023).
37. Youjian, S.; Min, Q. The Development and Applications of Foreign Offshore Cone Penetration Test Technology. *Urban Geotech. Investig. Surv.* **2022**, *192*, 199–204.
38. Robertson, P.K.; Robertson, K.L. *Guide to Cone Penetration Testing and Its Application to Geotechnical Engineering*; Gregg Drilling & Testing Inc.: Signal Hill, CA, USA, 2006.
39. Robertson, P.K. Interpretation of cone penetration tests—A unified approach. *Can. Geotech. J.* **2009**, *46*, 1337–1355. [CrossRef]
40. Fellenius, B.H.; Eslami, A. Soil profile interpreted from CPTu data. In Proceedings of the "Year 2000 Geotechnics" Geotechnical Engineering Conference, Asian Institute of Technology, Bangkok, Thailand, 27–30 November 2000.
41. Eslami, A.; Fellenius, B.H. Pile capacity by direct CPT and CPTu methods applied to 102 case histories. *Can. Geotech. J.* **1997**, *34*, 886–904. [CrossRef]

Disclaimer/Publisher's Note: The statements, opinions and data contained in all publications are solely those of the individual author(s) and contributor(s) and not of MDPI and/or the editor(s). MDPI and/or the editor(s) disclaim responsibility for any injury to people or property resulting from any ideas, methods, instructions or products referred to in the content.